Measured Admittance Model for Dynamic Simulation of Inverter-Based Resources Using Numerical Laplace Transform

Miao Zhang*, Li Bao*, Zhixin Miao*, Lingling Fan *, Pablo Gomez†,
*Department of Electrical Engineering
University of South Florida
Tampa FL 33620
†Department of Electrical and Computer Engineering
Western Michigan University
Kalamazoo MI 49008
Email: linglingfan@usf.edu

***Abstract*—With confidentiality constraints of detailed control information of inverter-based resources (IBR), black-box models, e.g., admittance/impedance models, obtained from measurements are often used for stability analysis. This paper makes a further inquiry: If stability analysis is possible with admittance models, is it possible to produce time-domain simulation results with admittance models only? One method adopted in the literature is to create a linear state-space model for the entire system by interconnecting components. The requirement for such an approach is that each component's model should be proper. To relax this requirement, the current paper seeks an alternate approach: direct conversion of frequency-domain data to time-domain data via numerical Laplace transform (NLT). To begin with, this paper presents NLT's advantage over inverse fast Fourier transfer (IFFT) using tutorial examples. This is followed by an example of a type-4 wind farm weak grid operation stability analysis and fast simulation using admittance models obtained from measurements. It can be seen that frequency-domain measurements, along with data fitting and NLT, lead to not only stability analysis but also fast time-domain simulation for stability demonstration.**

***Index Terms*—Numerical Laplace transform; inverter-based resources; admittance model; Fourier transform; transient analysis; oscillations.**

I. Introduction

Higher inverter-based resources (IBR) penetration can lead to many stability issues in real world, e.g., low-frequency oscillation observed in type-4 wind farms with weak grid interconnection [1]–[3] and subsynchronous resonances (SSR) in type-3 wind farms when integrated to series compensation [4].

IBR's converter control info is technology proprietary. Hence, the majority of the white box models used for IBR in the literature, e.g., [5], [6], are based on speculation. To tackle grid integration stability issues for a specific wind farm or solar PV farm, black-box models, i.e., impedance or admittance models, obtained from measurements, are generally used [7]. Frequency scanning method [8] and transient response measurement-based tools [9], [10] are usually adopted to measure the IBR's admittance.

Frequency scans results in each IBR's admittance frequency-domain measurement. Frequency-domain data fitting methods, e.g., vector fitting [11], further convert the measurement data into an s-domain model or a Laplace transfer function matrix. The s-domain admittance model enables stability analysis via closed-loop system eigenvalues [12].

In this paper, we investigate how to carry out fast time-domain simulation using the s-domain admittance models.

Obviously, a critical step is to obtain the entire system's model, in s-domain or in linear state-space format. The linear state-space format is preferred in the literature. Component connection method (CCM) has been used by research groups [13], [14] and consulting firms [15].

The CCM treats each component as a linear state-space model with input and output specified. The entire system will be created by interconnecting the components. A strict requirement is that each component should have a proper model. For example, $R + Ls$ is not a proper model since it has more zeros than poles. Therefore, special manipulation is required for each case.

We approach the problem by a different method: direct conversion of frequency-domain data to time-domain data. Inverse fast Fourier transform (IFFT) is known for this function; however, it has certain practical limitations (which will be shown in Section III). Therefore, NLT will be adopted for this goal.

With a given or measured impedance/admittance model, this paper will introduce how to conduct fast time-domain simulation.

For demonstration, a system of a type-4 wind farm with a parallel connected STATCOM is used as an example. The admittances of the wind farm and the STATCOM are first identified via frequency scans. Their DQ admittance models are estimated from measured data through vector fitting. Next, the whole system's admittance model is obtained. Finally, the system time-domain responses are obtained using an NLT routine. The proposed approach leads to an efficient and sim-

ple method of time-domain simulation-based demonstration with frequency-domain measurement data given. Compared to electromagnetic transient (EMT) testbed-based simulation, this approach is very fast. [16] discussed the computational burden benefits of NLT approach.

The rest of this paper is organized as follows. Section II introduces the NLT routine briefly. Section III presents two simple electric circuits as examples to illustrate the limitation of IFFT method. Section IV presents the process of transforming the frequency-domain data to time-domain data for the test system. Finally, conclusions are drawn in Section V.

II. NLT Routine

In this section, numerical Laplace transform (NLT) implementation will be introduced briefly. The reader can refer to [17] for the details and coding.

The input data of NLT computation is equally-sampled frequency-domain data, while the output is time-domain data.

For a given Laplace transfer function, e.g., $F(s)$, we may set N as the total number of samples in the time domain, and T as the observation time. The sampling intervals for frequency-domain and time-domain discretization are $\Delta\omega$ and Δt, respectively, which can be computed as follows.

$$\Delta t = T/N, \;\; \Delta\omega = \pi/T \tag{1}$$

Using the intervals defined above, the discrete version of f(t) and F(s) are given as

$$f_n = f(n\Delta t), \quad \text{for } n = 0, 1, ...N-1 \tag{2}$$

$$F_{2k+1} = F(c + j(2k+1)\Delta\omega)), \quad \text{for } k = 0, 1, ...N-1 \tag{3}$$

where c is a damping coefficient [18], defined as follows:

$$c = \ln(N^2)/T \tag{4}$$

The inverse numerical Laplace transform is defined by (5).

$$f_n = \text{Re}\left\{ C_n \left[\sum_{k=0}^{N-1} F_{2k+1}\sigma_{2k+1} e^{j2\pi kn/N} \right] \right\} \tag{5}$$

where

$$C_n = 2Ne^{cn\Delta t} e^{j\pi n/N} \Delta\omega/\pi \tag{6}$$

The part inside the square bracket in (5) can be obtained from IFFT [19]. And the window function coefficient σ in (5) may adopt Hanning, Lanczos, and Blackman methods. The major MATLAB coding is attached in the appendix.

III. Examine NLT on Simple Circuits

This section presents two simple examples to illustrate IFFT and NLT application to transient analysis.

Fig. 1 shows a RLC circuit and a RL circuit in subplot (a) and (b), respectively. Assume $R = 0.3\ \Omega$, $L = 0.5/\omega_0$ H, and $C = 0.4/\omega_0$ F, where $\omega_0 = 377$ rad/s. Therefore, their Laplace admittance in s-domain can be written as follows:

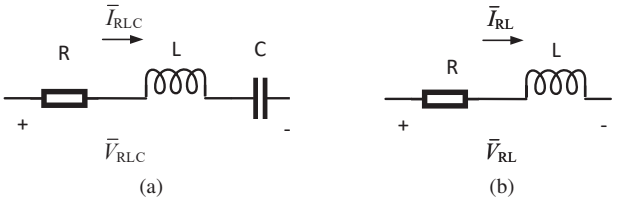

Fig. 1: RLC and RL circuit

$$Y_{RLC} = \frac{1}{R + Ls + \dfrac{1}{Cs}} \tag{7a}$$

$$Y_{RL} = \frac{1}{R + Ls} \tag{7b}$$

A step change will be applied to the source voltage. Bode plots of the current transfer function for the two circuits are presented in Fig. 2.

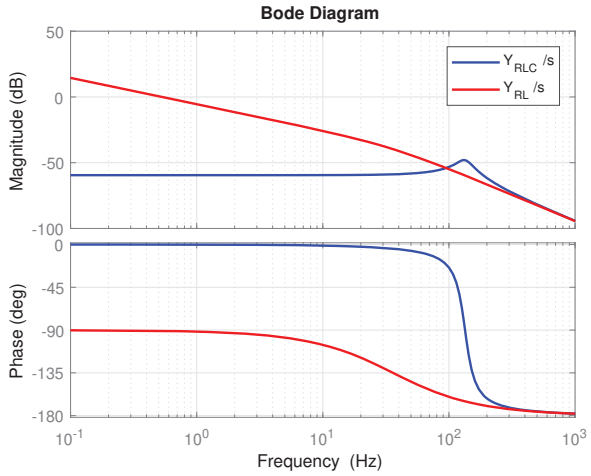

Fig. 2: Bode plots of (a) RLC and (b) RL circuit current response subject to a step change in the voltage: Y/s.

With the given Laplace-domain transfer functions and discretized frequency-domain data, the time-domain discrete data can be obtained via IFFT and NLT routine described in Section II. The computed time-domain response is compared with the transient responses obtained via MATLAB `step` function. All those time-domain data are plotted together in Fig. 3.

From Fig. 3 (a) RLC circuit, it can be observed that both IFFT and NLT methods can predict the exactly same time-domain transient responses as the benchmarked step response. From Fig. 3 (b), only NLT can produce the accurate time-domain data in the RL circuit example. IFFT's result does not match the actual time-domain response.

The reason for this discrepancy is that the RL circuit's frequency-domain data have no limit in the low-frequency range. This violates IFFT's assumption. NLT introduces damping into the conversion process; thus, NLT gives accurate time-domain results.

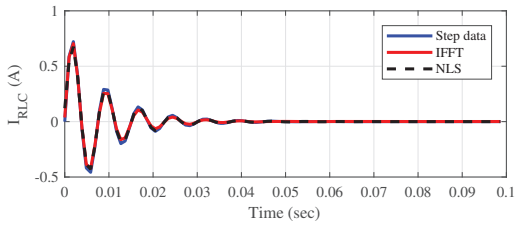

(a)

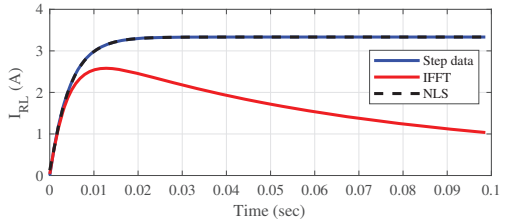

(b)

Fig. 3: Time-domain current response of (a) RLC circuit and (b) RL circuit.

IV. Test System of a Wind Farm with Weak Grid Interconnection

A type-4 wind farm with STATCOM is given in Fig. 4, which is built in MATLAB/SimPowerSystems platform. Assuming that wind and STATCOM control structures and parameters are unknown. We can treat them as two black-boxes and perform frequency scans to obtain the frequency-domain responses.

A. Admittance measurement

Fig. 5 shows the measurement test bed. The wind farm (or the STATCOM) are connected to a controllable voltage source. The fundamental components $V_{\mathrm{s,d0}}$ and $V_{\mathrm{s,q0}}$ ensure that the wind side operation condition is constant as in Fig. 4. At a frequency f_i, a 0.1 pu voltage harmonic injection ($V_{\mathrm{s,dinj}}$) is superimposed in the d-axis. Conversion between abc-frame and a 60-Hz dq-frame is based on the angle $\omega_0 t$. Next, the phasor at frequency f_i is extracted via Fourier transform from the measured current in the dq-frame. The admittance left column $Y_{\mathrm{wind,dd}}(f_i)$ and $Y_{\mathrm{wind,qd}}(f_i)$ are computed by the ratios of current phasors against voltage phasors in the dq frame. Similarly, another harmonic injection at q-axis voltage ($V_{\mathrm{q,inj}}$) and measured dq currents can identify the right column component $Y_{\mathrm{wind,dq}}(f_i)$ and $Y_{\mathrm{wind,qq}}(f_i)$. Hence, the measured wind side admittance at frequency f_i can be written as (8). The measurement range is from 1 Hz to 100 Hz with 1 Hz interval, and measured data are shown as the red markers in Fig. 6.

$$Y_{\mathrm{wind}}(f_i) = \begin{bmatrix} Y_{\mathrm{wind,dd}}(f_i) & Y_{\mathrm{wind,dq}}(f_i) \\ Y_{\mathrm{wind,qd}}(f_i) & Y_{\mathrm{wind,qq}}(f_i) \end{bmatrix} = \begin{bmatrix} \dfrac{I_{\mathrm{s,d}}(f_i)}{V_{\mathrm{s,d}}(f_i)} & \dfrac{I_{\mathrm{s,d}}(f_i)}{V_{\mathrm{s,q}}(f_i)} \\ \dfrac{I_{\mathrm{s,q}}(f_i)}{V_{\mathrm{s,d}}(f_i)} & \dfrac{I_{\mathrm{s,q}}(f_i)}{V_{\mathrm{s,q}}(f_i)} \end{bmatrix} \tag{8}$$

After obtaining the measurement data in the frequency-domain, vector fitting [11] is implemented to find the s-domain transfer function for the wind farm admittance. The blue lines in Fig. 6 show the vector fitting results, which match the measured data very well. Note that the order is set to 14 in vector fitting computation. $Y_{\mathrm{wind}}(s)$ and $Y_{\mathrm{STAT}}(s)$ represent the wind and STATCOM admittance s-domain transfer functions.

An RL circuit is used to represent the grid side network. X_g indicates the grid inductance in p.u. and $R_g = 0.1X_g$. Hence, the grid side admittance s-domain transfer function can be expressed as:

$$Y_{\mathrm{g}}(s) = \begin{bmatrix} Y_{\mathrm{g,dd}}(s) & Y_{\mathrm{g,dq}}(s) \\ Y_{\mathrm{g,qd}}(s) & Y_{\mathrm{g,qq}}(s) \end{bmatrix} = \begin{bmatrix} R_g + Ls & -L\omega_0 \\ L\omega_0 & R_g + Ls \end{bmatrix}^{-1} \tag{9}$$

The total admittance of the wind system with and without STATCOM can be derived via the following equations:

$$Y_{\mathrm{tot}}(s) = Y_{\mathrm{wind}}(s) + Y_{\mathrm{g}}(s) \tag{10a}$$

$$Y_{\mathrm{tot}}(s) = Y_{\mathrm{wind}}(s) + Y_{\mathrm{STAT}}(s) + Y_{\mathrm{g}}(s) \tag{10b}$$

B. Eigenvalue analysis

Eigenvalues of the complete system can be obtained using `tzero`$(Y_{\mathrm{tot}}(s))$ in MATLAB. Eigenvalue trajectory with varying grid impedance X_g from 0.3 to 0.5 p.u. is presented in Fig. 7. For the system without the STATCOM, it can be seen that there is a 10-Hz mode crossing the imaginary-axis when X_g increases to 0.42 p.u. On the other hand, a 4-Hz mode will move to the right-half-plane (RHP) after adding the STATCOM when X_g is greater than 0.4 p.u. Thus, we can predict that this wind farm system without STATCOM will experience 10-Hz oscillations, and the wind farm system with STATCOM will experience 4-Hz oscillations when the grid becomes weak.

C. Time-domain transient responses

With the total admittance model, the system impedance can be found by equation (11).

$$Z_{\mathrm{tot}}(s) = Y_{\mathrm{tot}}(s)^{-1} = \begin{bmatrix} Z_{\mathrm{tot,dd}}(s) & Z_{\mathrm{tot,dq}}(s) \\ Z_{\mathrm{tot,qd}}(s) & Z_{\mathrm{tot,qq}}(s) \end{bmatrix} \tag{11}$$

The total system impedance reflects the relationship between the PCC voltage and the current injection to the PCC voltage:

$$\begin{bmatrix} \Delta V_{\mathrm{d}} \\ \Delta V_{\mathrm{q}} \end{bmatrix} = \begin{bmatrix} Z_{\mathrm{tot,dd}}(s) & Z_{\mathrm{tot,dq}}(s) \\ Z_{\mathrm{tot,qd}}(s) & Z_{\mathrm{tot,qq}}(s) \end{bmatrix} \begin{bmatrix} \Delta I_{\mathrm{d}} \\ \Delta I_{\mathrm{q}} \end{bmatrix} \tag{12}$$

The voltage dynamic responses subject to a step change in the d-axis (or q-axis) current injection can be found by evaluating NLT for each component of $Z_{\mathrm{tot}}(s)$. For example, for a step change in the d-axis current injection, the dq-axis voltages in s-domain are $Z_{\mathrm{tot,dd}}/s$ and $Z_{\mathrm{tot,qd}}/s$. The corresponding frequency-domain data can be directly converted to the time-domain responses via NLT. In Fig. 8, (1) indicates I_{d} step change and (2) indicates I_{q} step change.

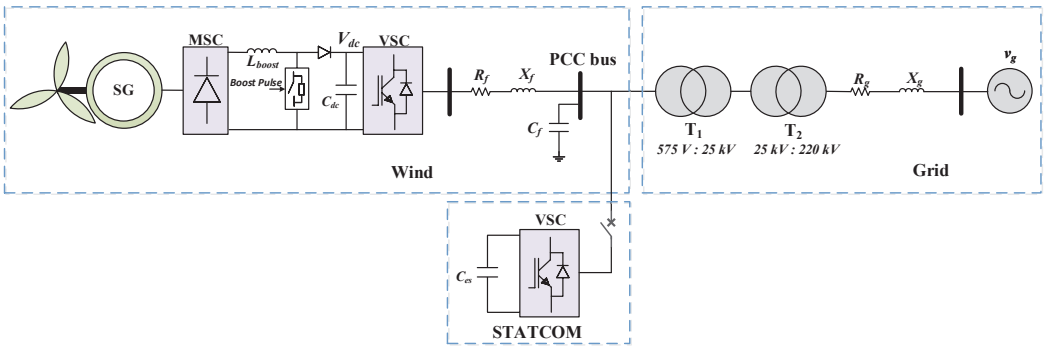

Fig. 4: EMT test bed of a type-4 wind farm with a STATCOM in MATLAB/SimPowerSystems

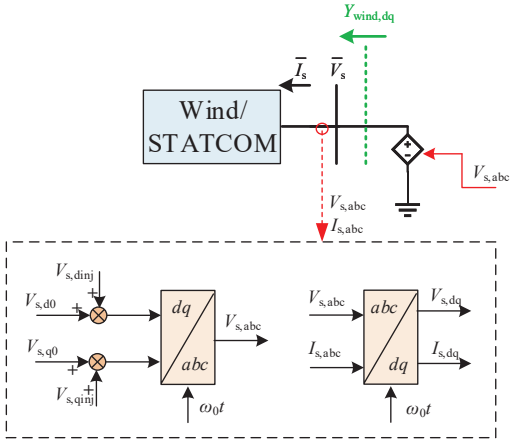

Fig. 5: Wind/STATCOM admittance measurement using frequency scanning method in dq-frame.

Fig. 8 (a) presents the scenario without STATCOM. Blue lines represents the case when $X_g = 0.42$ p.u. Red lines correspond to $X_g = 0.38$ p.u. The system has undamped 10-Hz oscillations when X_g is 0.42. If X_g is 0.38, the 10-Hz oscillations have more damping. This matches the eigenvalue analysis results in Fig. 7 (a).

Additionally, there are 100-Hz oscillations quickly damped in both cases. That is due to the 100-Hz mode identified by the eigenvalue analysis. Similarly, the scenario with STATCOM is presented in Fig. 8 (b). It can be seen the 4-Hz oscillations occur once X_g is 0.44 p.u. The time-domain simulation results corroborate the eigenvalue analysis results in Fig. 7 (b).

To validate the NLT-based time-domain responses, the simulation results of the test bed from MATLAB/SimPowerSystems are presented in Fig. 9. Before $t = 1$ s, the grid-side impedance X_g is kept at 0.3 p.u. X_g has an increased value due to the tripping of a parallel transmission line at $t = 1$ s. Fig. 9 (a) presents the dynamic responses for the system without the STATCOM. It shows that the wind system will have 9-Hz undamped oscillations if X_g increases to 0.42 p.u. On the other hand, Fig. 9 (b) presents the dynamic responses for the system with the STATCOM. Once X_g is increased above 0.42 p.u, there will be 3.5-Hz undamped oscillations. Those observations agree with the fast time-domain dynamic responses obtained from NLT routine, shown in Fig. 8.

V. Conclusion

This paper illustrates how to implement the NLT routine to carry out fast time-domain simulation based on admittance models obtained from measurements. Firstly, the paper demonstrates the advantage of NLT over IFFT through two simple examples. Secondly, the paper offers an alternate approach of fast time-domain simulation starting from admittance models. While the prior art, e.g., CCM, relies on converting an admittance model to a linear state-space model and interconnecting various components to a closed-loop system, the proposed approach directly deals with s-domain admittance models and leads to a closed-loop system expressed in s-domain. Time-domain simulation results are obtained through direct conversion of frequency-domain data to time-domain data. This approach is straightforward. The approach has been tested on a grid-interconnected type-4 wind farm to demonstrate weak grid oscillations with and without STATCOM.

References

[1] S.-H. Huang, J. Schmall, J. Conto, J. Adams, Y. Zhang, and C. Carter, "Voltage control challenges on weak grids with high penetration of wind generation: Ercot experience," in *2012 IEEE Power and Energy Society General Meeting*. IEEE, 2012, pp. 1–7.

[2] L. Fan, "Modeling type-4 wind in weak grids," *IEEE Transactions on Sustainable Energy*, vol. 10, no. 2, pp. 853–864, 2018.

[3] L. Fan and Z. Miao, "Wind in weak grids: 4 hz or 30 hz oscillations?" *IEEE Transactions on Power Systems*, vol. 33, no. 5, pp. 5803–5804, 2018.

[4] X. Xie, X. Zhang, H. Liu, H. Liu, Y. Li, and C. Zhang, "Characteristic analysis of subsynchronous resonance in practical wind farms connected to series-compensated transmissions," *IEEE Transactions on Energy Conversion*, vol. 32, no. 3, pp. 1117–1126, 2017.

[5] M. Zhang, Z. Miao, and L. Fan, "Reduced-order analytical model of grid-connected solar photovoltaic system for low-frequency oscillation analysis," *IEEE Transactions on Sustainable Energy*, 2021.

[6] Y. Xu, M. Zhang, L. Fan, and Z. Miao, "Small-signal stability analysis of type-4 wind in series-compensated networks," *IEEE Transactions on Energy Conversion*, vol. 35, no. 1, pp. 529–538, 2019.

[7] S. Shah, P. Koralewicz, V. Gevorgian, H. Liu, and J. Fu, "Impedance methods for analyzing stability impacts of inverter-based resources: Stability analysis tools for modern power systems," *IEEE Electrification Magazine*, vol. 9, no. 1, pp. 53–65, 2021.

[8] B. Badrzadeh, M. Sahni, Y. Zhou, D. Muthumuni, and A. Gole, "General methodology for analysis of sub-synchronous interaction in wind power plants," *IEEE Transactions on Power Systems*, vol. 28, no. 2, pp. 1858–1869, 2012.

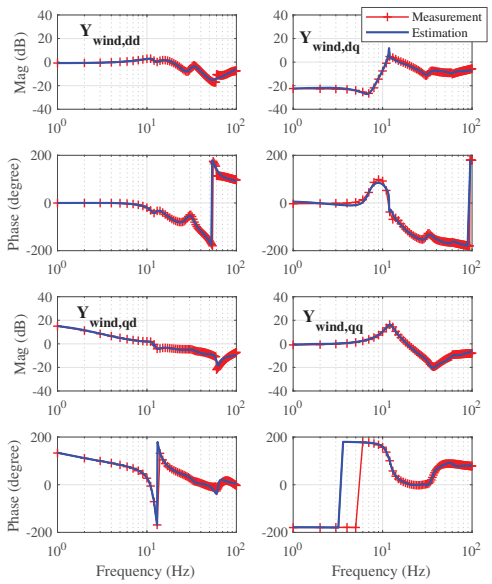

(a)

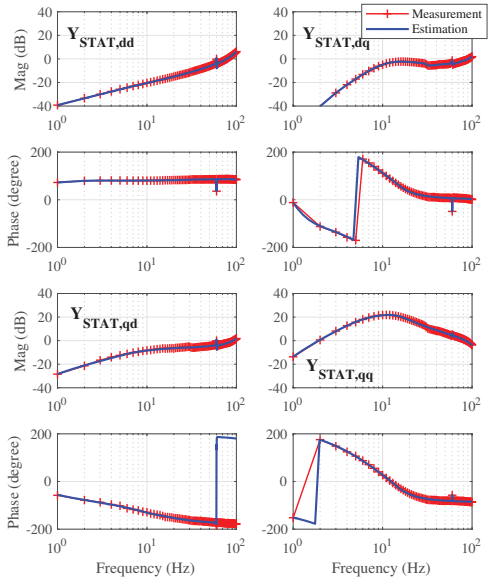

(b)

Fig. 6: (a) Wind and (b) STATCOM admittance frequency responses in *dq*-frame.

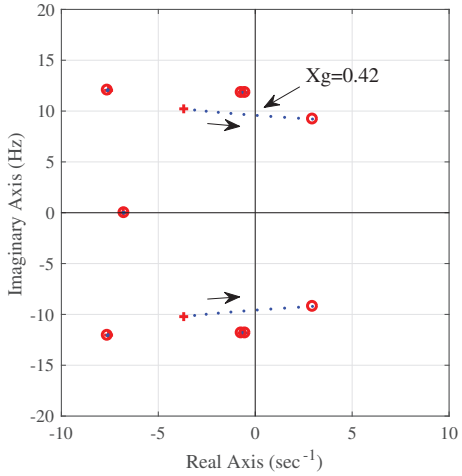

(a)

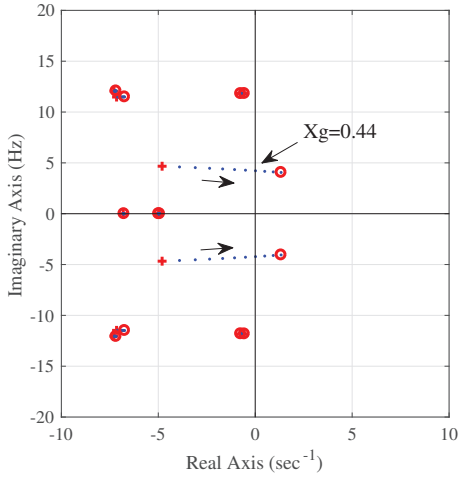

(b)

Fig. 7: Eigenvalue trajectory when varying X_g from 0.3 to 0.5 p.u. with 0.02 step interval. (a) without STATCOM; (b) with STATCOM.

[9] J. Huang, K. A. Corzine, and M. Belkhayat, "Small-signal impedance measurement of power-electronics-based ac power systems using line-to-line current injection," *IEEE Transactions on Power Electronics*, vol. 24, no. 2, pp. 445–455, 2009.

[10] L. Fan and Z. Miao, "Time-domain measurement-based *dq*-frame admittance model identification for inverter-based resources," *IEEE Transactions on Power Systems*, vol. 36, no. 3, pp. 2211–2221, 2020.

[11] B. Gustavsen and A. Semlyen, "Rational approximation of frequency domain responses by vector fitting," *IEEE Transactions on power delivery*, vol. 14, no. 3, pp. 1052–1061, 1999.

[12] L. Fan and Z. Miao, "Admittance-based stability analysis: Bode plots, nyquist diagrams or eigenvalue analysis?" *IEEE Transactions on Power Systems*, vol. 35, no. 4, pp. 3312–3315, 2020.

[13] Y. Wang, X. Wang, Z. Chen, and F. Blaabjerg, "Small-signal stability analysis of inverter-fed power systems using component connection method," *IEEE Transactions on Smart Grid*, vol. 9, no. 5, pp. 5301–5310, 2017.

[14] Y. Wang, X. Wang, F. Blaabjerg, and Z. Chen, "Harmonic stability analysis of inverter-fed power systems using component connection method," in *2016 IEEE 8th International Power Electronics and Motion Control Conference (IPEMC-ECCE Asia)*. IEEE, 2016, pp. 2667–2674.

[15] M. K. Das and A. M. Kulkarni, "Inclusion of frequency scanning based dq models of facts and hvdc systems in large scale eigen-value analysis programs for analysis of torsional interactions," in *13th IET International Conference on AC and DC Power Transmission (ACDC 2017)*, 2017, pp. 1–6.

[16] G. Bilal, P. Gomez, R. Salcedo, and J. M. Villanueva-Ramirez, "Electromagnetic transient studies of large distribution systems using frequency domain modeling methods and network reduction techniques," *International Journal of Electrical Power & Energy Systems*, vol. 110, pp. 11–20, 2019.

[17] P. Moreno and A. Ramirez, "Implementation of the numerical laplace transform: A review task force on frequency domain methods for emt studies, working group on modeling and analysis of system transients using digital simulation, general systems subcommittee, ieee power engineering society," *IEEE Transactions on power delivery*, vol. 23, no. 4, pp. 2599–2609, 2008.

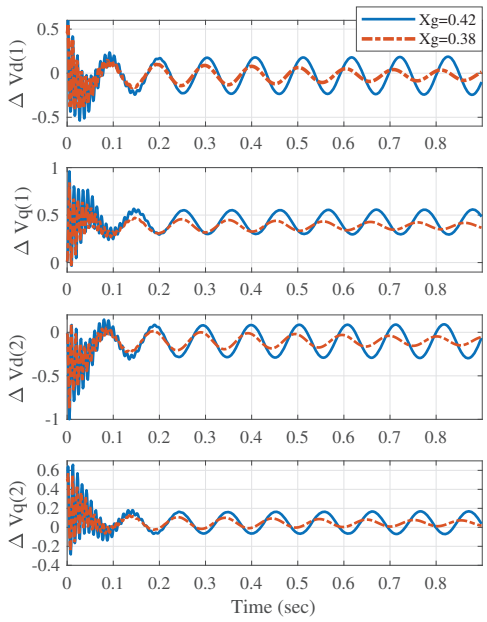

(a)

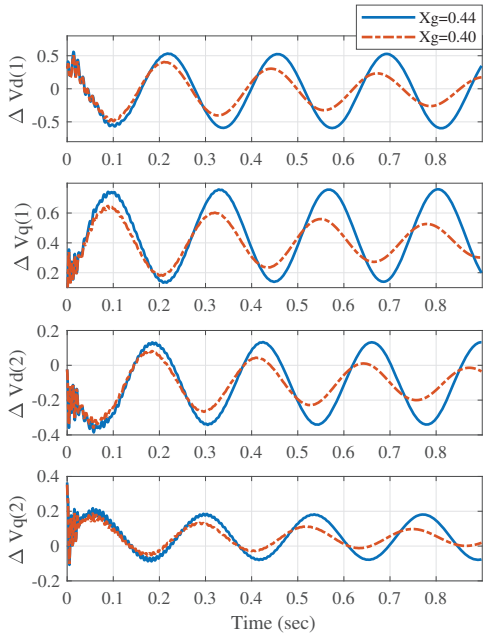

(b)

Fig. 8: NLT derived voltage time-domain response regarding current step injection on PCC bus. (a) wind farm without STATCOM. (b) wind farm with STATCOM.

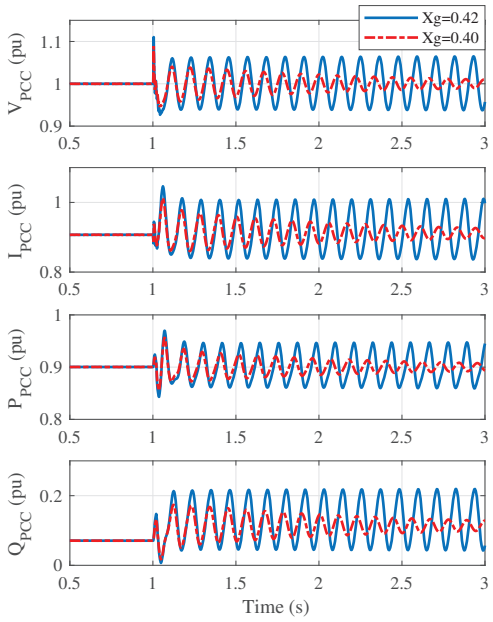

(a)

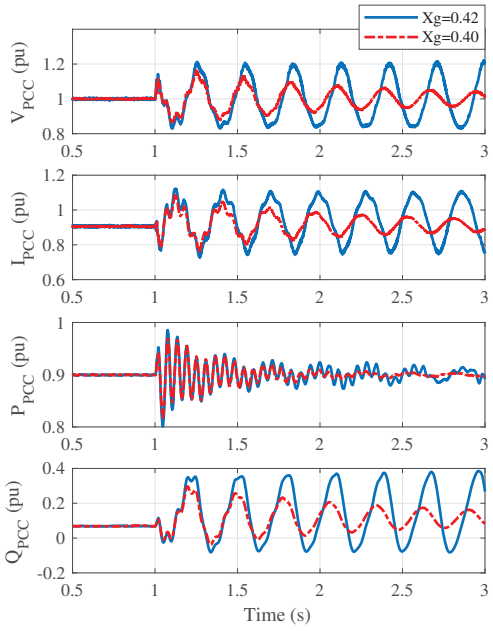

(b)

Fig. 9: EMT time-domain simulation regarding tripping a transmission line. All initial condition is when $X_g = 0.3$ p.u. (a) without STATCOM. (b) with STATCOM.

[18] L. Wedepohl, "Power system transients: Errors incurred in the numerical inversion of the laplace transform," in *Proc. of the 26th Midwest Symposium on Circuits and Systems*, 1983.

[19] J. G. Proakis, *Digital signal processing: principles algorithms and applications*. Pearson Education India, 2001.

APPENDIX

MATLAB Code

```
c = log(N^2)/T; % damping coefficient
Cn = (2*N*dw/pi)*exp(c*dt+1i*pi/N).^n;
% Blackman window function
sigma = 0.42 +0.5*cos(0.5*pi*m/N) +...
        0.08*cos(pi*m/N);
% Fs is discrete frequency-domain responses
% ftd is discrete time-domain responses
Fs = Fs.*sigma;
ftd = ifft(Fs);
ftd = real(Cn.*ftd);
```